Antimony sorption and removal on carbon steel/magnetite surfaces in relation to pressurized heavy water reactors

S. J. Keny[1], A. G. Kumbhar[1,*], A. Sanjukta[2], S. Pandey[2], S. Ramanathan[3] and G. Venkateswaran[2]

[1]Water and Steam Chemistry Division, [2]Analytical Chemistry Division, and
[3]Material Science Division, Bhabha Atomic Research Centre, Mumbai 400 085, India

In nuclear power plants corrosion and activation of structural material and its re-deposition on out-of-core surfaces is of significance as far as structural integrity and radiation exposure to the employees are concerned. Recently, Indian Pressurized Heavy Water Reactors have faced a typical problem of activation of antimony (Sb) from primary heat transport pump seals containing ~10% Sb. This Sb cannot be removed easily and its deposition mechanism is yet to be clearly understood. This article deals with studies related to the understanding of this process and a solution for the removal of Sb.

Keywords: Antimony, absorption and removal, carbon steel, magnetite, pressurized heavy water reactors.

COMPONENT integrity and radiation dose to employees are two important factors for safe and economic operation of a nuclear power plant. Problem of radiation exposure due to activated antimony (Sb) has arisen in some of the nuclear power plants[1]. Radioactive antimony isotopes (^{122}Sb and ^{124}Sb) are the cause of radiation field in the primary coolant systems[2]. In the Pressurized Heavy Water Reactors (PHWRs) coolant pumps of the primary heat transport (PHT) system operate at 563 K temperature and 12 MPa pressure. Pump seals and bearings of the pump contain antimony-impregnated graphite[3,4]. Due to these aggressive conditions, traces of Sb come into the PHT system by erosion/corrosion either in ionic or sub-micron particulate form. Under the reducing conditions of PHT and radiation-induced reduction[5], Sb ionic form can be reduced to lower oxidation state or to metallic nanoparticles. Thus, circulation and/or deposition of Sb on zircaloy surfaces inside the core of the nuclear reactor take place. Neutron flux present in the reactor core activates ^{121}Sb and ^{123}Sb to radioactive isotopes ^{122}Sb ($t_{1/2}$ 2.6 days) and ^{124}Sb ($t_{1/2}$ 60 days) respectively, by n, γ reaction. Part of this activated ^{122}Sb and ^{124}Sb gets released and is deposited on the magnetite-coated carbon steel (CS) surface outside the core or on steam generator tube surfaces due to various mechanisms like surface charges, ion exchange, physical sorption, etc.[6,7]. The release of Sb activities from reactor core occurs during the draining of steam generator and the header-level control operation carried out at the time of reactor shutdown. This may be due to the possibility of Sb(III) oxidation to Sb(V) by air ingress in the system. The exact chemical condition that leads to the release of antimony has not been clearly established in PHWRs. Oxygen ingress during shutdown operations is cited as one of the reasons. However, Sb species and their oxidation state present on zircaloy surfaces in the reactor core is not well known[8,9].

In the case of PHWRs, magnetite is the prominent oxide on the CS surfaces as reducing water chemistry is employed. The active Sb released from the reactor core deposits on the outer CS piping surfaces of the PHT system, thereby increasing the radiation fields and resulting in exposure to the station personnel and person-sivert (man-rem) expenditure during maintenance work. Once Sb gets deposited on bare CS surfaces or magnetite-bearing CS surfaces, it is not amenable for removal by reductive decontamination process. It has to decay by its own half-life or has to be removed by oxidative dissolution. Oxidative treatment for antimony removal[10] may not be compatible with the PHWR system. Hence, it is important to understand the phenomenon of Sb deposition on CS surfaces and its removal during decontamination of PHT system of PHWRs in reducing water chemistry condition.

Magnetite is also a chemically stable material and has been used for removing heavy metals (like Sb) in the pH range 9.5–10.5 from wastewater by metal ferrite formation method[11]. Temperature, reaction time, pH, concentration and type of metal ion (species) have been reported to have effects on this process[12–14]. The reductive decontamination process suffers from quick Sb re-deposition on the magnetite surface. To have an insight into the above process, Sb-doped magnetite was prepared and characterized by X-ray diffraction and X-ray photoelectron spectroscopy and the point of zero charge (PZC) was determined[15]. The absorption of Sb on carbon steel surface was studied. The oxide dissolution in two

*For correspondence. (e-mail: agk@barc.gov.in)

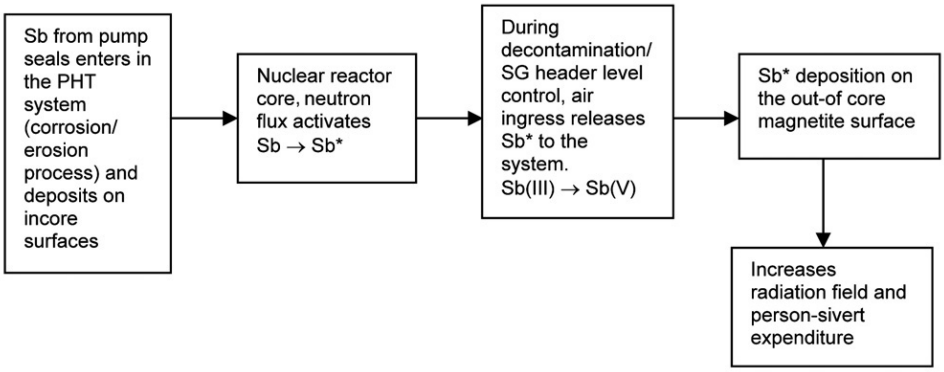

Figure 1. Schematic of Sb activation and re-deposition mechanism in PHWRs.

decontamination formulations was studied for comparison. They are: (1) CEA: C = citric acid (1.4 mM); E = EDTA = ethylenediaminetetraacetic acid (1.4 mM), A = ascorbic acid (1.7 mM). (2) CEG: C (1.4 mM); E (1.4 mM); G = gallic acid (1.7 mM).

Only CA refers to citric acid, GA refers to gallic acid and AA refers to ascorbic acid.

CEG formulation was found to be better than CEA for decontamination as Sb absorption was inhibited in CEG significantly. The Sb ingress in reactor core, activation and re-deposition mechanism in PHWRs is schematically shown in Figure 1. Details of the above studies are given in this article.

Experiments

Materials and method

Magnetite doped with 1%, 2% and 5% Sb was synthesized by co-precipitation method. $Fe(OH)_2$ and $Sb(OH)_3$ were co-precipitated from ferrous ammonium sulphate and antimony trichloride ($SbCl_3$) by adding alkali (NaOH) under controlled nitrogen atmosphere. The co-precipitate was digested on a hot water-bath for ~4 h. The precipitate was then filtered; washed with nano pure water and wet precipitate was transferred to the furnace and heated at 1173 K for 12 h in an inert atmosphere. The powder X-ray diffraction (XRD) pattern of the oxide sample was recorded using a Philips X-ray diffractometer with CuK_α as the X-ray source and Ni filter over a monochromator. X-ray photoelectron spectra (XPS) were recorded using VG Scientific spectrometer.

Oxide dissolution experiments were carried out in 200 ml CEA and CEG formulation at 353 K in a magnetically stirred, thermostated glass vessel. The amount of oxide corresponding to 4 mM Fe was subjected to dissolution at pH 2.8 in de-oxygenated atmosphere, keeping a steady-state flow of nitrogen. Samples were withdrawn periodically and filtered through 0.2 μm paper. Dissolved Fe concentration in the filtrate was determined using UV–Visible spectrophotometer by ortho-phenanthroline method[16]. Sb was estimated by using ICP-MS (VG – PQ Excell, VG Elemental, UK).

Next, 0.5 g magnetite powder was dispersed in 25 ml water and CEG and CEA formulations. The pH of the solutions was adjusted to 1.5, 3.0, 4.0, 5.0, 6.0, 6.5, 7.0 and 8.0 with 0.1 N HNO_3 or KOH and ionic strength was adjusted at 0.1 M with KNO_3. The PZC values were determined by using Zeta Sizer-3000 (M/s Malvern).

Circular CS coupons of 15.1 mm dia and 1.2 mm thick were sequentially polished up to 600 grade and exposed to 563 K in a solution of pH 10.2 (maintained by LiOH) in an autoclave. This is to simulate PHT system conditions of PHWR to some extent. XRD analysis of the oxide film scrapped from the CS specimen indicated that the film was made of magnetite[17].

CS, magnetite powder and magnetite-coated CS coupons were independently exposed to CEA and CEG formulations containing 25 mg/l of Sb at 353 K, while stirring the solution on a magnetic stirrer and Sb sorption was studied.

Results and discussion

Oxide characterization

Figure 2 shows the XRD patterns of magnetite and antimony trioxide (Sb_2O_3) along with 1%, 2% and 5% Sb-doped magnetite (JCPDS 85–1436). Sb_2O_3 has X-ray diffraction at $2\theta = 28.55$ and 25.67. XRD patterns of 1% and 2% antimony-doped magnetite are similar to those of pure magnetite (fcc). In the case of 5% Sb-doped magnetite along with the pure magnetite XRD pattern, two additional peaks were observed at $2\theta = 28.41$ and 24.14. The presence of Sb_2O_3 peaks in the case of 5% Sb-doped magnetite along with the pure magnetite peaks shows biphasic nature. This indicates the formation of solid solution up to 2% Sb doping with magnetite. At 5% Sb doping, a mixture is formed rather than solid solution. The large shift in peak position corresponding to magnetite

phase towards the higher angle suggests the incorporation of Sb^{5+} (0.060 pm) than Sb^{3+} (0.056 pm). The incorporation of Sb^{5+} into the lattice is likely to cause further cation vacancy leading to the lattice contraction. The observed unit cell parameters are shown in Table 1. The saturation limit of Sb doping in Fe_3O_4 is 1%.

Figure 3 *a* shows XPS peaks of $Sb3d_{3/2}$, $Sb3d_{5/2}$ and Figure 3 *b* shows XPS peaks of $Fe2p_{3/2}$ from the 2% antimony-doped magnetite. $Fe2p_{3/2}$ photoelectron peaks are analysed to know the chemical state of Fe in antimony-doped magnetite for the chemical interaction. The binding energy of $Fe2p_{3/2}$ is 711.2 eV, indicating that Fe is predominantly in +3 states. Absence of a significant shoulder at the lower binding-energy side of this peak excludes the possibility of Fe^{2+} state. The principal $Sb3d_{3/2}$, $Sb3d_{5/2}$ XPS peaks have binding energies 529.59 and 539.35 eV respectively. Absence of any peak or shoulder at the lower energy side of these peaks indicates that Sb was seen to be in the oxidized state. It is difficult to distinguish between Sb^{+3} and Sb^{+5} because the difference of their binding energy is too small (only ~0.3 eV)[18]. Thus, it can be inferred that at low doping levels, $Sb^{+3/+5}$ ions incorporate in the magnetite lattice.

Dissolution of antimony doped magnetite

Figures 4 and 5 show plots of Fe and Sb dissolved in CEA and CEG formulations as a function of time during dissolution of Sb-doped magnetite respectively. For both Sb and Fe dissolution rates were higher for CEA than CEG.

In earlier studies similar dissolution trends for Fe_3O_4 and α-Fe_2O_3 were observed in different formulations[19]. In the initial 100 min Sb-doped magnetite showed twice faster dissolution for Fe compared to Sb. Dissolution proceeds in two stages: (a) faster initial stage up to 50–70% dissolution, and (b) second stage with lower dissolution rate setting in after the first stage with increasing antimony content in magnetite. In the case of GA-based formulation, it is a single-step dissolution with respect to both Fe and Sb. The cause for lower dissolution rate could be primarily due to the presence of antimony in the oxide, decreased particle surface area to volume ratio due to agglomeration[20,21], and depletion in reagent concentration. With increase in Sb concentration in the doped magnetite, the dissolution rate becomes slower in the GA-based CEG formulation (Table 2). XRD pattern (Figure 2) of antimony-doped magnetite clearly shows that antimony in the oxide remains as a separate oxide phase at 5% Sb doping. Hence at and beyond 5% doping, the excess antimony may exist in the oxide as separate Sb_2O_3. This may be hindering the dissolution process, resulting in slow dissolution at higher Sb doping.

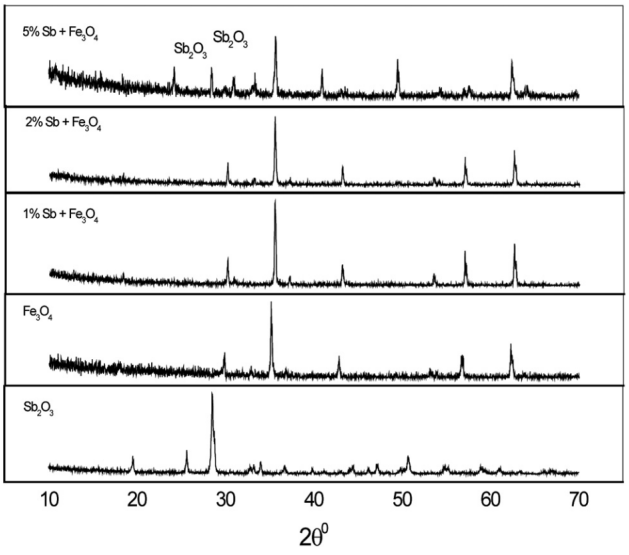

Figure 2. XRD patterns of pure magnetite, antimony oxide and 1%, 2% and 5% antimony-doped magnetite.

Point of zero charge studies of oxides

PZC of a suspended particle in a medium is the pH of the medium at which particle surface charge (zeta potential) is zero. It gives an idea about the surface charge of a particle in a particular medium and hence its interaction with other charged surfaces. PZC values of Sb-substituted magnetite (Figure 6) were determined to know in what way it can be adsorbed on the reactor internal surfaces. Zeta potential measurements were carried out by dispersing solid oxide powder in liquid medium of varying pH at constant ionic strength (0.1 M). Table 3 shows PZC values of various oxides in aqueous medium and formulations. In aqueous medium PZC values of Fe_3O_4 and Sb_2O_3 were 6.5 and 1.7 respectively. In GA-based CEG formulations for magnetite, PZC was 2.5. Charge on both the oxides changed from positive to negative with the increase in pH, as higher pH facilitates the deprotonation of M–OH functional groups. As is evident from Table 3, the PZC of 2% Sb-doped magnetite in simple aqueous medium (PZC = 4.6) was higher than that in the decontamination formulation (PZC = 1.5). Hence at pH 4, surface charge on Sb-doped magnetite was negative in the formulation and positive in the aqueous solution. In AA-based CEA formulation up to pH 1.5, the surface charge was negative and hence even at this low pH, the PZC value could not be reached. This indicated existence of

Table 1. Unit cell parameters

Compound	Cell parameter (Å)	Cell volume (Å^3)
Fe_3O_4 (pure)	8.44	601.4
1% Sb-doped Fe_3O_4	8.37	585.8
2% Sb-doped Fe_3O_4	8.37	585.7

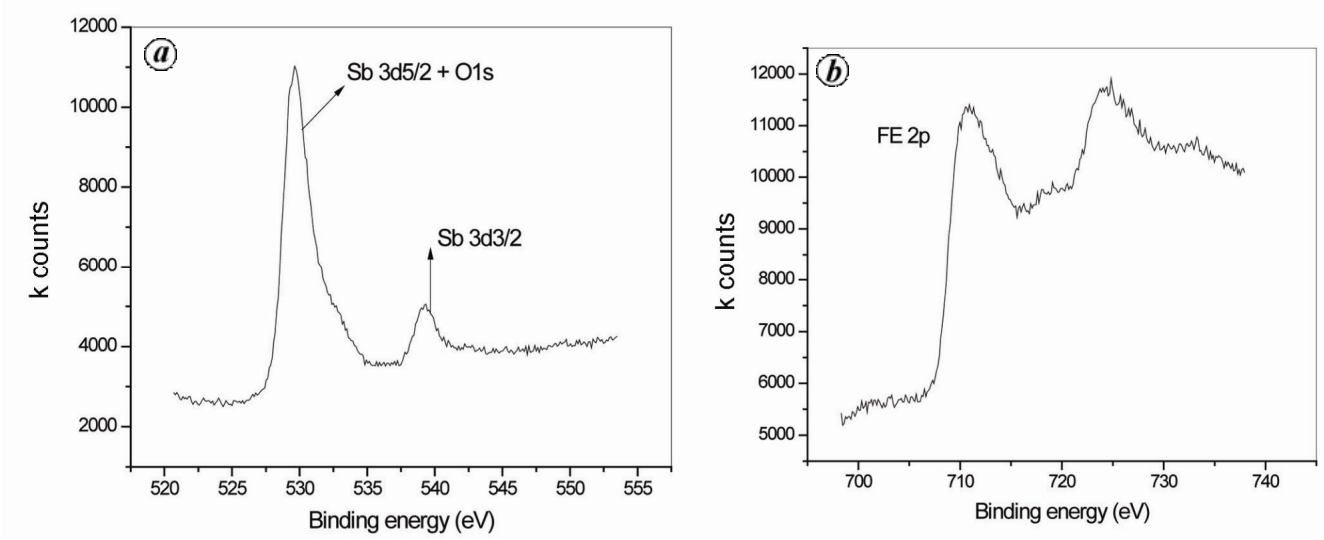

Figure 3. ***a***, $Sb3d_{3/2}$, $Sb3d_{5/2}$ photoelectron peaks from the antimony-doped magnetite. ***b***, $Fe2P_{3/2}$ photoelectron peak from the antimony-doped magnetite.

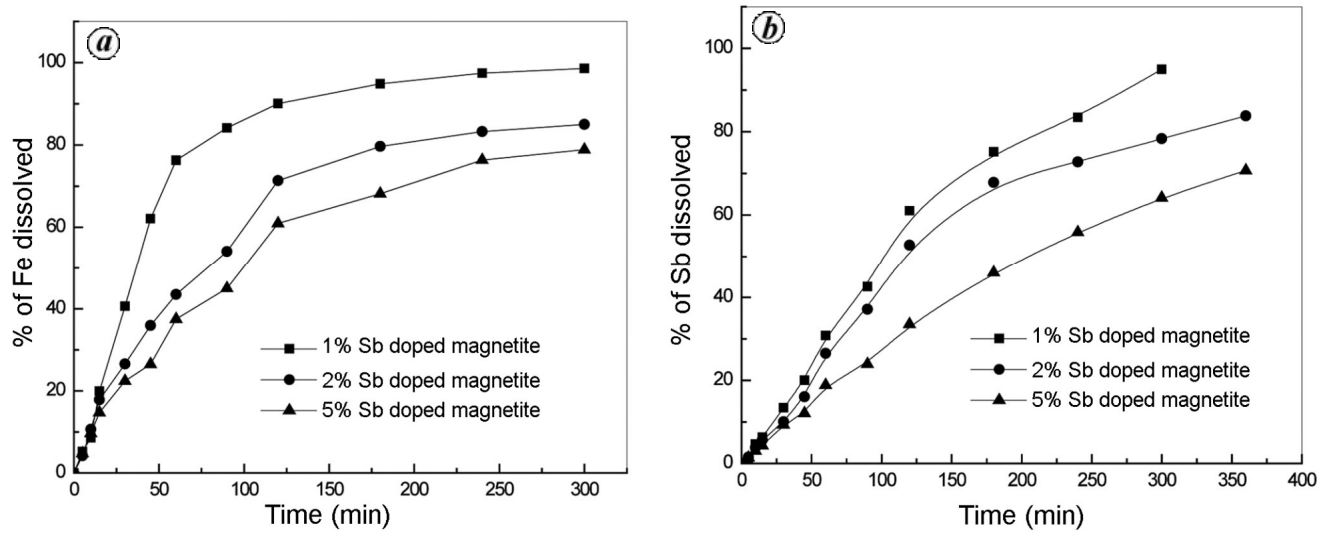

Figure 4. Percentage dissolution with time of antimony-doped Fe_3O_4 in CA + EDTA + AA formulation (1.4 + 1.4 + 1.7) mM: ***a***, Percentage of Fe released. ***b***, Percentage of antimony released.

Table 2. Rate constants (min^{-1}) for dissolution of antimony-doped Fe_3O_4 in CA + EDTA + AA/GA (1.4 + 1.4 + 1.7) mM formulation

Oxides and dissolution formulations	% Fe released	% Sb released	K (min^{-1}) for Fe	K (min^{-1}) for Sb
Magnetite	99.8	–	2.5×10^{-2}	–
1% Sb-doped magnetite CEA (CA + EDTA + AA)	98.56	95.01	[a]6.48×10^{-3} [b]1.39×10^{-3}	[a]1.90×10^{-3} [b]1.94×10^{-3}
2% Sb-doped magnetite CEA	85.04	83.8	[a]2.54×10^{-3} [b]7.009×10^{-4}	[a]1.59×10^{-3} [b]9.48×10^{-4}
5% Sb-doped magnetite CA + EDTA + AA	78.87	70.72	[a]1.98×10^{-3} [b]7.79×10^{-4}	[a]9.76×10^{-4}
1% Sb-doped magnetite CEG (CA + EDTA + GA)	82.43	78.24	[a]2.36×10^{-3}	[a]1.25×10^{-3}
2% Sb-doped magnetite CEG	76.91	72.83	[a]1.43×10^{-3}	[a]1.08×10^{-3}
5% Sb-doped magnetite CEG	69.55	66.32	[a]9.35×10^{-4}	[a]8.37×10^{-4}

[a]First stage, [b]Second stage.

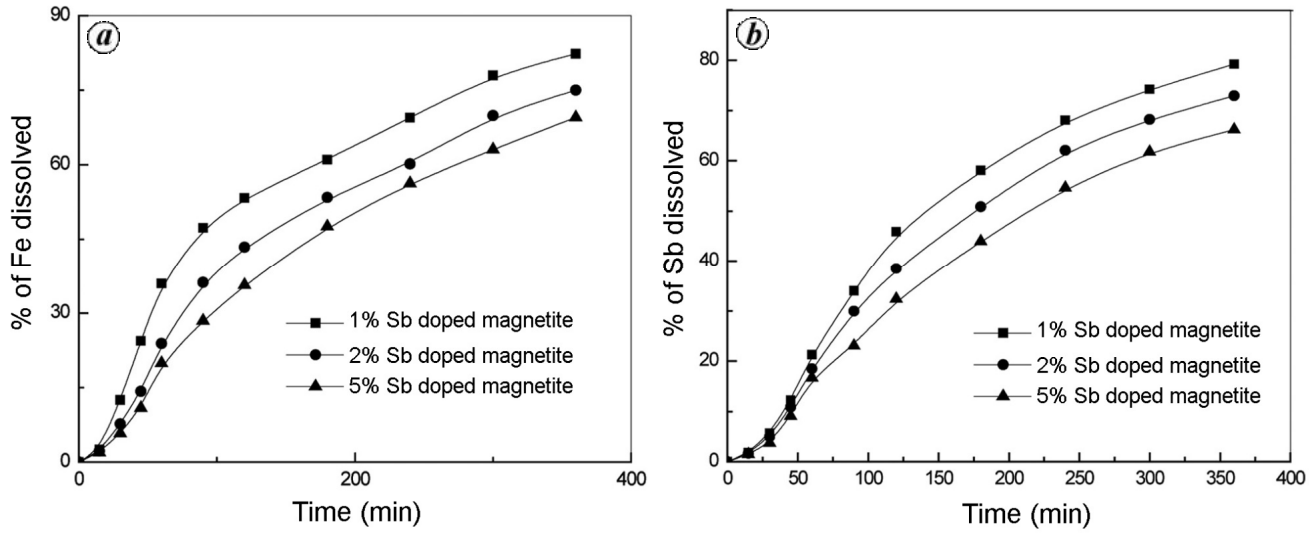

Figure 5. Percentage dissolution with time of antimony-doped Fe_3O_4 in CA + EDTA + GA formulation (1.4 + 1.4 + 1.7) mM: (***a***) Percentage of Fe released. (***b***) Percentage of antimony released.

Table 3. Point of zero charge (PZC) of different oxides in decontamination formulation and in aqueous medium

Oxides	Formulations	PZC
Sb_2O_3	Water	1.7
Sb-doped Fe_3O_4	Water	4.6
Fe_3O_4	Water	6.5
Fe_3O_4	CEG (CA + EDTA + GA)	2.5
Sb-doped Fe_3O_4	CEG	1.5

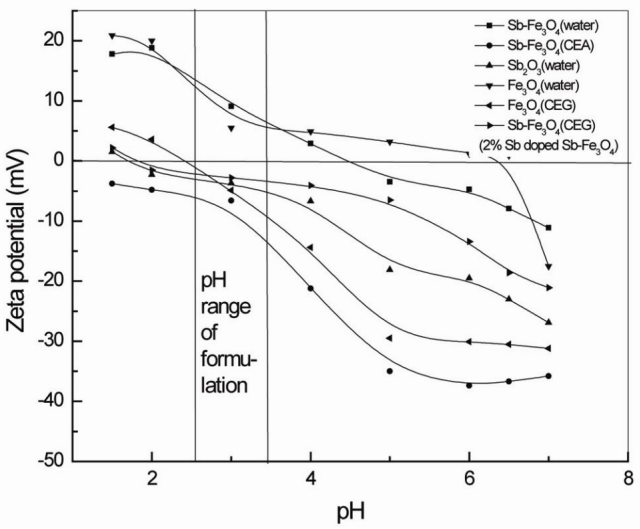

Figure 6. Zeta potential of magnetite and antimony-doped magnetite in aqueous medium as well as in the formulations at various pH values.

strong negative surface charge on Sb-doped magnetite in AA-based CEA formulation, whose initial pH values are in the range 2.5–3.0. The charge arises from the protonation/deprotonation of surface hydroxyl groups bonding to Fe and Sb atoms resulting in Sb–OH and Fe–OH surface functional groups. The surface hydroxyls can be protonated or deprotonated, depending on the pH of the suspension and the PZC of the oxides. It can be seen from Figure 6 that in the pH range 2.0–2.5, which is close to the pH range 2.5–3.0 of the decontamination formulations employed in this study, there is a surface charge transition from negative to positive. Particularly magnetite surface retains a weakly negative charge or no charge, while Sb-doped magnetite tends to be strongly negatively charged. Thus in GA-based (CA + EDTA + GA) formulation both magnetite and Sb-doped magnetite have similar negative charge. By virtue of this there can be an electrostatic repulsion and the magnetite-bearing CS surface may not favour the sorption of Sb-doped magnetite in this medium.

Sorption of Sb on carbon steel surface

CS coupons, magnetite-coated CS coupons and magnetite powder were exposed to CEG and CEA formulations at pH 2.8 under deaerated conditions containing 25 ppm concentration of Sb^{+3} or Sb^{+5} to study the Sb sorption. Figure 7 shows the plot of antimony remaining in the solution as a function of time. In Table 4 saturation Sb sorption values are given. In CEG formulation there is no sorption of Sb^{+5} on the CS coupons. Whereas for Sb^{+3} in CEG formulation during the first 1–2 h of exposure, there was rapid sorption on the CS coupons, resulting in 65% sorption. After 2 h exposure, a steady state concentration of about 45–50% of initial concentration of Sb taken was observed in solution, which indicates some leaching out

of sorbed Sb from the CS surface. There was around 55% concentration of antimony in the solution (i.e. 45% sorption) after about 6 h of exposure. Magnetite-coated CS coupons exposed to CEG formulation containing 25 ppm concentration of Sb^{+3}, showed 50% Sb sorption.

In the case of magnetite powder exposed to CEG formulation, there was hardly 13% sorption of Sb^{+3}. CEA formulation containing a strong reducing agent like AA showed almost complete Sb sorption on CS. As AA is a good reducing agent, it may be enabling the conversion Sb^{+3} to Sb with the help of electrons release by Fe corrosion from CS thus enhancing the deposition of Sb on CS as shown below. In the equations given below, ascorbic acid is represented by H_2A and its oxidation product is represented by A*.

$$2Fe \rightarrow 2Fe^{+2} + 4e^-, \quad E^0 = 0.44V \text{ (vs SHE)}.$$
$$4H_2A \rightarrow 4A^* + 8H^+ + 8e^-, \quad E^0 = -0.45 \text{ V (vs SHE)}.$$
$$4SbO_2^- + 16H^+ + 12e^- \rightarrow 4Sb + 8H_2O.$$

$$2Fe + 4H_2A + 4SbO_2^- + 8H^+ \rightarrow 4A + 2Fe^{+2} + 4Sb + 8H_2O.$$

Thus the deposition of Sb in the presence of AA must be followed by the release of Fe^{+2} from CS. Under reducing conditions, Sb^{+3} sorbs more strongly on Fe^{+3} hydroxides than Sb^{+5} and Sb^{+3} solubility is also much lower than that of Sb^{+5} species[6,22]. However, in GA-based formulation, no deposition of Sb^{+5} was observed on magnetite powder and on CS surface. Sb^{+3} showed approximately 40% deposition on CS surface and magnetite-bearing CS surface. Complete adsorption of Sb^{+3} was observed on CS surface in the AA-based formulation.

AA is a strong reducing agent and reduces Fe^{+3} ions in the oxide lattice or Fe(III)-L complex both by inner sphere and outer sphere electron transfer pathway to form Fe^{+2} ions and Fe(II)-L complex. Fe dissolved in the presence of 25 ppm Sb^{3+} was found to be more in CEA than in CEG medium as shown in Figure 8. The complexing ability of the solution results in the reduced metal ion released as Fe(II)-L complex in the solution and Sb ion gets sorbed on the oxide lattice resulting into complete sorption of Sb. The mechanism can be represented as follows:

$$\{-Fe^{+3}\}_{oxide} + [Fe(II) - EDTA]_{(aq)}^{-2} \rightarrow$$

$$\underset{\text{(Sorption of Fe(II)EDTA complex on oxide)}}{\{Fe^{+3}...Fe(II) - EDTA\}_{oxide}} \rightarrow$$

$$X\underset{\text{(Intramolercular e-transfer)}}{\{Fe^{+2}...Fe(II) - EDTA\}_{oxide}} \xrightarrow{EDTA_{(aq)}}$$

$$[Fe(II) - EDTA]_{(aq)}^{-2} + [Fe(II) - EDTA]_{(aq)}^{-} \rightarrow$$

Further continuation of this process.

GA is a strong reducing agent compared to AA, but it did not result in a significant reduction of Fe^{3+} of the oxide lattice[23]. The electron charge transfer path to Fe^{3+} seems to be hindered due to its specific aromatic nature,

Table 4. Adsorption of Sb^{+3} on carbon steel (CS), magnetite-coated CS and magnetite powder under different conditions

Material	Formulation	Concentration (mM)	Sorption of Sb^{+3} %
Magnetite powder	CEG (CA + EDTA + GA)	1.4 + 1.4 + 4	13.2
Carbon steel (CS)	CEG	1.4 + 1.4 + 4	40.0
Magnetite-bearing CS	CEG	1.4 + 1.4 + 4	50.6
CS	CA + EDTA	4 + 2	91.2
CS	CEA	1.4 + 1.4 + 2	100

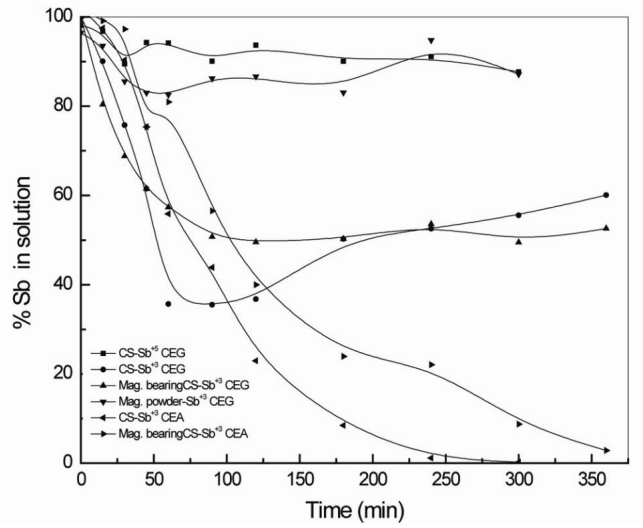

Figure 7. Sorption of antimony on carbon steel (CS) coupons in various formulations.

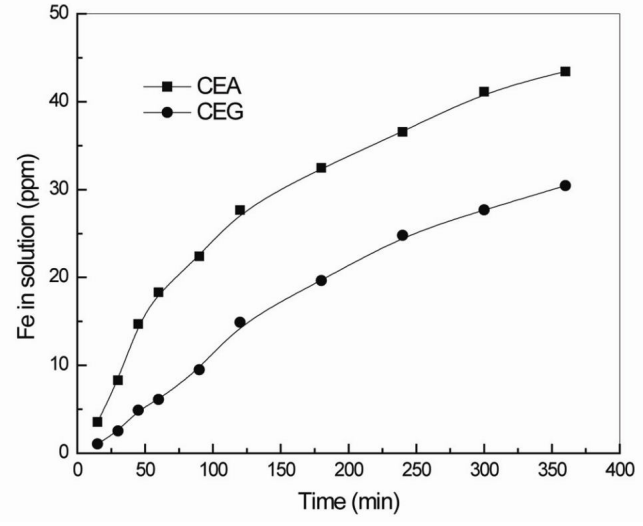

Figure 8. Dissolution of Fe (vs time) from CS surface in the presence of 25 ppm Sb^{+3} in CEA and CEG media.

resulting in insignificant sorption of Sb. Such an effect of GA seems to reduce Sb sorption on the oxide lattice compared to AA. Thus, AA presents a favourable condition for the reduction of Fe^{3+} to Fe^{2+}, and yielding complete sorption of Sb.

$$\{-Fe^{+3}\}_{oxide} + H_4Y \rightarrow \{-Fe^{+3}\}_{oxide} \ldots H_3Y^- + H^+.$$
$$2\{-Fe^{+3}\}_{oxide} \ldots H_3Y^- \rightarrow 2\{Fe^{+2}\ldots\}_{oxide} + \text{Quinone} + 2H^+.$$
$$2\{Fe^{2+}\ldots\}_{oxide} + 2\ EDTA_{(aq)} \rightarrow 2\ [Fe(II) - EDTA]^{2-}_{(aq)}.$$

Conclusions

The adsorption of antimony on CS, magnetite-coated CS surface and magnetite powder has been studied. Gallic acid-based formulation prevents Sb deposition on CS/magnetite surface to great extent. Whereas in AA-based formulation complete sorption of Sb on CS was observed and sorption of Sb on magnetite surface seems to be hindered to some extent. XPS data indicate lattice substitution of Sb^{+3} for Fe^{+2} in magnetite at low doping levels ($\leq$5%). These studies indicate that CEG formulation is a better decontamination formulation where Sb activity problems are encountered than CEA and may be preferred as it results in optimum oxide dissolution and lower Sb sorption.

1. Velmurugan, S. *et al.*, Experience with antimony activity removal processes in Indian PHWRS. In Proceedings of Symposium on Operational and Environmental Issues Concerning use of Water as a Coolant in Power Plants and Industries (OPENWAC 2008), Kalpakkam, December 2008, p. 86.
2. Velmurugan, S., Rufus, A. L., Sathyaseelan, V. S., Subramanian, V., Mittal, V. K. and Narasimhan, S. V., Experience with dilute chemical decontamination in Indian pressurized heavy water reactors. *Energy Proc.*, 2011, **7**, 645–649.
3. Anderson, C. G., The metallurgy of antimony. *Chem. Erde*, 2012, **72**(S4), 3–8.
4. Varrica, D., Bardelli, F., Dongarra, G. and Tamburo, E., Speciation of Sb in airborne particulate matter, vehicle break linings, and break pad wear residue. *Atmos. Environ.*, 2013, **64**, 18–24.
5. Hanglein, A., Reactions of organic free radicles at colloidal silver in aqueous solution. Electron pool effect and water decomposition. *J. Phys. Chem.*, 1997, **83**(17), 2209–2216.
6. Satoshi, M., Yoshio, T. and Yasuko, T., μ-XANES evidence for reduction of Sb(V) to Sb(III) in soil from Sb mine tailing. *Environ. Sci. Technol.*, 2010, **44**, 1281–1287.
7. Satoshi, M., Yoshio, T., Yasuko, T. and Masahiro, S., Antimony(V) incorporation into synthetic ferrihydrite, geothite, and natural iron oxyhydroxides. *Sci. Technol.*, 2010, **44**, 3712–3718.
8. Mittal, V. K., Bera, S., Velmurugan, S. and Narasimhan, S. V., Studies on sorption of antimony on carbon steel surface in chemical decontamination medium. *J. Nucl. Sci. Technol.*, 2011, **48**(2), 256–262.
9. Mittal, V. K., Antimony adsorption and its inhibition on carbon steel and magnetite surfaces in chemical decontamination process. Ph D thesis submitted to Homi Bhabha National Institute, Mumbai, 2013.
10. Dundar, Y., Odar, S., Streit, K., Allsop, H. and Guzonas, D., Application of KWU antimony removal process at Gentilly-2. In proceedings of Water Chemistry of Nuclear Reactor Systems, BNES-7, Berlin, 1996, pp. 266–268.
11. Shin-jo, Kim, Mitsuru, A., Tamura, M. and Suzuki, Y., A study on antimony-bearing ferrites. *J. Hazard. Mater.*, 1998, **57**, 1–12.
12. Mandaokar, S. S., Dharmadhikari, D. M. and Dara, S. S., Retrival of heavy metal ions from solution via fertilization. *Environ. Pollut.*, 1994, **83**, 277–282.
13. Kondoh, M., Nakashima, N. and Hirasawa, T. J., Characteristics of heavy metal dissolution from Zn, Gd and Mn bearing ferrites *Jpn. Soc. Water Environ.*, 1992, **5**, 313–320.
14. Tamaura, Y., Katsura, T., Rojarayanont, S., Yoshida, T. and Abe, H., Ferrite process, heavy metal ions treatment system. *Water Sci. Technol.*, 1991, **23**, 1893–1900.
15. Parks, G. A., The isoelectric points of solid oxides, solid hydroxides and aqueous hydroxo complex system. *Chem. Rev.*, 1965, **65**(2), 177–198.
16. Vogel, A. I., *A Textbook of Quantitative Inorganic Analysis including Elementary Instrumental Analysis*, ELBS and Longman, London, 1982, 3rd edn, p. 787.
17. Prince, A. A. M., Velmurugan, S., Narasimhan, S. V., Ramesh, C., Murugesan, N., Raghavan, P. S. and Gopalan, R., Dissolution behaviour of magnetite film formed over carbon steel in dilute organic acid media. *J. Nucl. Mater.*, 2001, **289**(3), 281–290.
18. Allen, M. D., Poulston, S., Bithell, E. G., Goringer, M. J. and Bowker, M., An XPS, TEM and TPD study of the oxidation and ammoxidation of propene using mixed Fe–Sb oxide catalysts. *J. Catal.*, 1996, **163**, 204–214.
19. Keny, S. J., Kumbhar, A. G., Venkateswaran, G. and Kishore, K., Radiation effects on the dissolution kinetics of magnetite and hematite in EDTA- and NTA-based dilute chemical decontamination formulations. *Radiat. Phys. Chem.*, 2005, **72**, 475–482.
20. Nii, K. and Hisamatsu, Y., The relation between the rate of dissolution and the surface area: study on zinc ferrite. *Trans. Natl. Res. Inst. Met.*, 1964, **6**(4), 26–30.
21. Segal, M. G. and Sellers, R. M., Kinetics of metal oxide dissolution: reductive dissolution of nickel ferrite by tris (picolinato) vanadium(II). *J. Chem. Soc. Faraday Trans. I*, 1982, **78**, 1149–1164.
22. Kirch, R., Scheinost, A. C., Rossberg, A., Banerjee, D. and Charlet, L., Reduction of antimony by nano-particulate magnetite and mackinawite. *Mineral. Magaz.*, 2008, **72**(1), 27–30.
23. Keny, S. J., Kumbhar, A. G., Thinaharan, C. and Venkateswaran, G., Gallic acid as a corrosion inhibitor of carbon steel in chemical decontamination formulation. *Corros. Sci.*, 2008, **50**, 411–419.

ACKNOWLEDGEMENTS. We thank Dr T. Mukherjee (Ex. Director, Chemistry Group, BARC) and Dr S. V. Narasimhan (Ex. Associate Director and Head, Water and Steam Chemistry Division (WSCD), BARC) for encouragement during this study. We also thank Dr S. Velmurugan (Head, WSCD, BARC) for valuable discussions, and Shri Mohsin Jafar, Dr S. N. Achary and Dr A. K. Tyagi for help in XRD data analysis.

Received 20 February 2013; revised accepted 21 February 2014